Effect of Volute Collector on the Performance of Centrifugal Pump Based on Entropy Generation Analysis

Maitrik Shah[*], Beena Baloni, Salim Channiwala

Department of Mechanical Engineering, Sardar Vallabhbhai National Institute of Technology, Gujarat, India

Abstract

A proper design of centrifugal pumps reduces power loss and improves efficiency. This study aims to investigate and analyze the effect of different volute collector configurations on centrifugal pump performance. Locations of losses are detected using the entropy production rate, whereas the number of losses is evaluated using user-defined codes. Three volute collectors are selected based on their connections with standard pipes. A steady flow numerical analysis is performed to determine the performance parameters of the centrifugal pump and select a modified volute collector design. Comparing the results of experiments on the base and modified volute collectors confirmed that the proper design of the volute collector can help reduce the secondary flow losses at subsequent locations, which reduces the entropy production and losses. As compared to the base pump, the modified volute collector improved the pump efficiency by 3% at the duty flow.

Keywords: centrifugal pump, entropy production, energy loss, volute collector

1. Introduction

Centrifugal pumps consume approximately 22% of the total standard electricity consumed by electric-powered motors globally; thus, they can significantly help in energy savings [1-2]. Single-stage radial flow centrifugal pumps with a medium head and flow are widely used in processing, agricultural, and industrial projects. Proper design of the centrifugal pumps with upstream and downstream pipe connections reduces the power loss and improves their efficiency. Computational fluid dynamics (CFD) techniques help predict the performance characteristics of these pumps. Various studies have employed numerical and theoretical methodologies to evaluate the locations and mechanisms of loss production.

The entropy production theory explores unknown power losses. It locates local flow losses caused by the design structure under various operating conditions, which are difficult to investigate using experimental analyses. Kock and Herwig [3] proposed detailed CFD techniques for the entropy production in turbulent shear flows involving a heat transfer; first, they locally calculated the entropy production and subsequently integrated the entire flow domain. Bohle et al. [4] used Kock and Herwig's method to confirm that entropy production may be used to locate and identify high-loss areas in hydraulic machinery. Hongyu et al. [5] used the total pressure head difference at the inlet and outlet of the analyzed domain to calculate the head loss. They reported that the theoretical hydrodynamic performance was satisfactorily consistent with the experimental data of the tested centrifugal pump. Gu et al. [6] compared the measured power loss using entropy production and total pressure head difference methods. They detected significant flow losses owing to the clocking position of the vaned diffuser associated with the circular casing.

---

* Corresponding author. E-mail address: maitrikshah2006@gmail.com

Tel.: +91-972-5852858

Guan et al. [7] aimed to determine the causes and location of the energy loss; thus, they used the entropy production method to visualize the energy loss of a double-suction centrifugal pump at various flow rates. They claimed that the entropy production was primarily affected by the main flow regions that were themselves influenced by the volute design. The entropy production in the volute has a high proportion; even at a flow of 1.2 Qd, its contribution reaches 96%. Deng et al. [8] measured the energy loss using the impeller trimming method in a double-suction centrifugal pump. They identified a high energy dissipation loss near the volute tongue and in the volute diffuser. Simultaneously, Zhang et al. [9] applied the entropy production method to define flow losses inside the side-channel pump with different wrapping angles. Huang et al. [10] examined the energy loss owing to the direct turbulence and wall friction dissipation. They concluded that the turbulence and wall friction dissipation contribute significantly to entropy generation, whereas the volute contributes to the highest losses at different time steps.

Peng et al. [11] reported that in a slurry pump, the addition of a splitter blade after the impeller reduced the energy loss caused by the entropy. Yang et al. [12] calculated flow losses in a slanted axial-flow pump and proved that the entropy generation was the highest in the impeller. Li et al. [13] examined the flow characteristics and energy loss of a pump as a turbine. They reported that the asymmetric structure of the volute increased the hydraulic loss of downstream flow regions. Yang et al. [14] visualized flow losses in a vertical centrifugal pump using the entropy production method to achieve optimization in hydraulic components. Cui and Zhang [15] investigated energy losses in a straight-blade centrifugal pump and concluded that the energy was dissipated primarily owing to pressure pulsations and vibrations. Ji et al. [16] studied the energy characteristics of a mixed-flow pump with different impellers to guide the vane tip clearance. They concluded that the energy loss increased owing to the increment in the tip clearance, whereas the highest energy loss in the volute remained unchanged.

Therefore, significant energy losses at the volute diffusion section, impeller-volute clearance gap, volute tongue, and impeller blade inlet can be estimated using the calculated entropy production rate. A fluid motion inside the fluid domains dissipates irreversible mechanical energy during the conversion of the mechanical energy to hydraulic energy; this increases the entropy according to the second law of thermodynamics. The dissipated energy becomes accumulated in the pump assembly and pipe connections. Nonetheless, studies on the volute collector design considering the internal flow field and local energy losses are scarce. Moreover, the volute collector is a section after the volute tongue till the volute discharge diameter.

Consequently, the objective of this study is to identify the additional losses and reduce them in the fluid domain of a centrifugal pump with a provision of an appropriate volute collector design (area ratio). A centrifugal pump design with a nominal head, flow rate, and specific speed of 33 m, 0.03 m^3/s, and 134.53 (rpm, m^3/s, m), respectively, were considered. The volute collector inlet and outlet diameters of this pump assembly were 56.5 and 90 mm, respectively. Three different volute discharge diameters associated with standard pipe sizes of 90, 80, and 65 mm were chosen at volute collector area ratios of 40, 50, and 75%, termed as Vd-40, Vd-50, and Vd-75, respectively. First, the Ansys CFX software was used to conduct a numerical analysis. Based on the simulation results, the best configuration of the volute collector was experimentally explored and compared with the base configuration considering the performance parameters of the centrifugal pump.

2. Entropy Production Method

The governing equations of the conservation of mass, momentum, and energy were solved to explain the flow. The first law of thermodynamics was used to determine the energy equation in CFD. Kock and Herwig [3] used entropy as a direct parameter to calculate the efficiency of a technical system. They reported that the transmission of heat and pressure drop are connected in the entropy transport equation. In addition, they described two approaches for calculating the entropy production during the CFD simulation process. In this study, the direct method was considered. This method considers the entropy as a post-processing quantity, and the fluid is assumed incompressible with a minimal heat transfer in the hydraulic fluid machinery. Therefore, heat transfer is negligible, and the energy equation is not calculated.

According to the second law of thermodynamics, the specific entropy (s) variable grows in every physical system, and the time-averaged governing equation is as follows [3-6]:

$$\rho\left(\frac{\delta \overline{s}}{\delta t}+\overline{u}\frac{\delta \overline{s}}{\delta x}+\overline{v}\frac{\delta \overline{s}}{\delta y}+\overline{w}\frac{\delta \overline{s}}{\delta z}\right)=-\overline{div\frac{\overline{q}}{t}}-\rho\left(\overline{\frac{\delta u's'}{\delta x}}+\overline{\frac{\delta v's'}{\delta y}}+\overline{\frac{\delta w's'}{\delta z}}\right)+\overline{\left(\frac{\Phi}{T}\right)}+\overline{\left(\frac{\Phi_\theta}{T^2}\right)} \tag{1}$$

where the reversible heat transfer is denoted by $div\frac{\overline{q}}{t}=div\left(-\frac{\lambda}{T}gradT\right)$. This expression has no bearing on the assessment of flow losses. Furthermore, $\overline{\left(\frac{\Phi_\theta}{T^2}\right)}$ is an irreversible term formed by heat transfer; nevertheless, this term is rarely regarded in hydraulic machinery because thermal transmission is negligible. Fluid friction produces an irreversible term $\overline{\left(\frac{\Phi}{T}\right)}$, which is the only source of entropy in this study. The entropy induced by $\overline{\left(\frac{\Phi}{T}\right)}$ can be directly calculated in the CFD post-processing. As seen in Eq. (2) [3], flow losses produced by dissipation are principally caused by viscosity and turbulence that can be expressed as follows:

$$\overline{\left(\frac{\Phi}{T}\right)}=\frac{\Phi_{\overline{D}}}{\overline{T}}+\frac{\Phi_{D'}}{\overline{T}} \tag{2}$$

where $\frac{\Phi_{\overline{D}}}{\overline{T}}$ denotes that the entropy production rate is induced by viscous or direct dissipation. Using Eq. (3) [3], viscous dissipation may be directly estimated in the CFD post-processing.

$$\frac{\Phi_{\overline{D}}}{\overline{T}}=\frac{\mu}{\overline{T}}\left[2\left[\left(\frac{\partial \overline{u}}{\partial x}\right)^2+\left(\frac{\partial \overline{v}}{\partial y}\right)^2+\left(\frac{\partial \overline{w}}{\partial z}\right)^2\right]+\left(\frac{\partial \overline{v}}{\partial x}+\frac{\partial \overline{u}}{\partial y}\right)^2+\left(\frac{\partial \overline{w}}{\partial y}+\frac{\partial \overline{v}}{\partial z}\right)^2+\left(\frac{\partial \overline{u}}{\partial z}+\frac{\partial \overline{w}}{\partial x}\right)^2\right] \tag{3}$$

Entropy production through turbulent dissipation, also known as indirect dissipation, is described by the term on the right-hand side of Eq. (4) [3], as follows:

$$\frac{\Phi_{D'}}{\overline{T}}=\frac{\mu}{T}\left[2\left[\left(\frac{\partial u'}{\partial x}\right)^2+\left(\frac{\partial v'}{\partial y}\right)^2+\left(\frac{\partial w'}{\partial z}\right)^2\right]+\left(\frac{\partial v'}{\partial x}+\frac{\partial u'}{\partial y}\right)^2+\left(\frac{\partial w'}{\partial y}+\frac{\partial v'}{\partial z}\right)^2+\left(\frac{\partial u'}{\partial z}+\frac{\partial w'}{\partial x}\right)^2\right] \tag{4}$$

Because the fluctuating quantities are not available in the CFD solution based on the Reynolds-averaged-Navier-Stokes (RANS) equations, Eq. (4) cannot be solved directly. Some studies [3, 17] have provided the following equation to address this problem.

$$\frac{\Phi_{D'}}{\overline{T}}=\frac{\rho\varepsilon}{\overline{T}} \tag{5}$$

The accessible variable in the turbulence model, ε, is expressed as the dissipation rate of the turbulent kinetic energy. Finally, the power losses owing to the entropy formation can be calculated by integrating dissipations over the entire domain, as expressed in Eq. (6) [9]. The flow velocity gradient influences the entropy generation at the wall surface, and the wall shear dissipation is represented as Eq. (7) [18], where τ_w is the wall shear stress and v_w denotes the velocity near the wall (m/s). As for the total energy dissipation, Eq. (8) [18] is used to compute the total entropy production in the system.

$$P_{EP}=\int_v\left(\Phi_D+\Phi_{D'}\right)dV \tag{6}$$

$$P_w=\int_A\frac{\tau_w+v_w}{\overline{T}}dA \tag{7}$$

$$P_t=P_{EP}+P_w \tag{8}$$

The turbulence model and wall function influence the estimation of the turbulent and wall shear dissipations, respectively. Böhle et al. [19] revealed that the k-ε turbulence model predicts the maximum losses in the flow regions and exhibits a minimum variation with experimental results. In this study, a numerical analysis was performed with three different turbulence

models (RNG k–ε, k–ω, and k–ω SST), and their results were subsequently compared. In general, the RNG k–ε turbulence model yielded the maximum losses in the system and minimum variation with experimental data. Therefore, the RNG k–ε model was selected. The viscous dissipation value is considerably smaller than the turbulent dissipation value [10, 20], as discussed in the numerical result analysis. The power loss and location of loss production regions must be defined in machines. Some studies [4, 6] have introduced a dimensionless entropy production coefficient (EPC) Φ^*, which was calculated as follows:

$$\Phi^* = \frac{\left(\Phi_{\bar{D}} + \Phi_{D'}\right) d_2}{\omega^2 \rho Q} \tag{9}$$

EPC is determined using the volume flow rate Q, impeller outer diameter d_2, angular velocity ω, and the turbulent and viscous dissipations. It is used to compare the performance of machines under various operating situations.

3. Numerical Simulation

The centrifugal pump has a complex geometry structure; therefore, it is difficult to experimentally measure the associated variables. Different types of losses existing in all turbomachinery can be differentiated between internal and external losses. External losses are not considered in the CFD calculation; however, they can be calculated using a defined loss coefficient; external losses include bearings and shaft seal failures. Internal losses are considered in the CFD calculation; these include shock and friction losses. The term "dissipation" can be used to summarize various types of internal losses. The total losses of the system are a function of geometrical dimensions. The numerical simulation allows for the calculation of flow losses in machines that spatially and temporally depend on numerous study areas. A single-stage centrifugal pump, with a medium head of 33 m and flow rate of 0.03 m³/s, was selected as the simulation flow domain. The design parameters of the model pump are listed in Table 1.

Table 1 Centrifugal pump parameters

Parameters	d_1	d_2	b_1	b_2	β_1	β_2	φ	Z	δ	n_1	d_3	b_3	φ_o	d_4
Unit	(mm)	(mm)	(mm)	(mm)	(°)	(°)	(°)	(nos.)	(mm)	(mm)	(mm)	(mm)	(°)	(mm)
Value	100	172	30	28	28	22	117	6	5	10	189	56	24	90
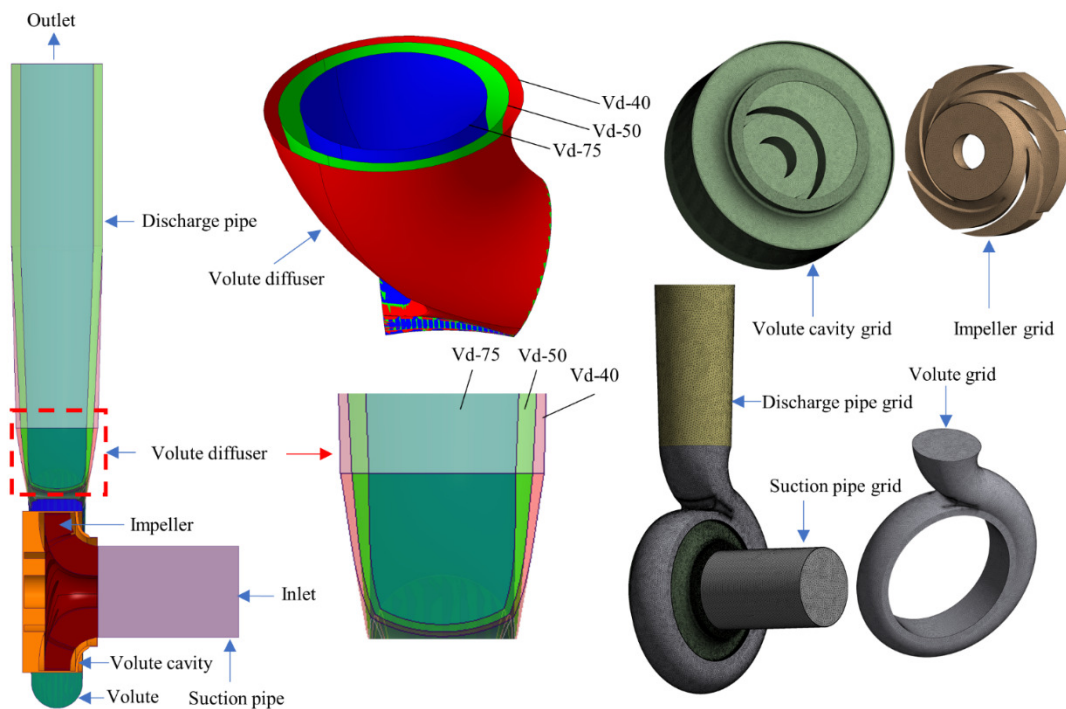
Fig. 1 Fluid domain of the centrifugal pump with volute collector configurations and grid profile

The Creo parametric software was used to build a numerical pump model consisting of extended suction and discharge line, impeller, volute, and volute cavity, as shown in Fig. 1. The computational grid was generated for the designed geometry to define the energy loss and predict the location, intensity, and operating regimes for flow appearance in fluid domains. The unstructured mesh was used for meshing, as shown in Fig. 1. The patch confirming method with tetrahedral mesh was selected for meshing. The element quality >0.2, skewness <0.75, and orthogonal quality >0.25 were maintained in the developed grid. An inflation layer meshing with a first-layer wall thickness was used to capture the boundary layer region for any wall-bounded turbulent flow. The inflation layer mesh can accurately predict the near-wall velocity [21]. The quality of the mesh near the wall directly affects the friction loss, and a highly refined mesh increases the mesh skewness. The tri-linear shape function for tetrahedral elements was used for numerical discretization [22]. The numerical and experimental results were reasonably consistent for a Y^+ value below 60, whereas the upper limit of Y^+ for the pump was 300 [21].

To improve the accuracy of the results and reduce the computational time of numerical simulations, the grid independence test was conducted at a nominal flow rate with the same solver setup. The grid refinement was verified with six different mesh counts in the range of 3.6-10.5 M and corrected with the head and efficiency of the pump, as presented in Table 2. The data presented in the table reveals that an increase in grid numbers decreases the percentage error in the performance parameters [10, 12]. Additionally, the percentage error was less than 1 when the grid size was more than 8.5 M. As refining, the mesh with more grid numbers requires more computational time and does not necessarily provide a unique solution for increasing the accuracy of the results [21], a grid size of 10.5 M was selected in the numerical analysis. The grid numbers and Y^+ values of each domain are listed in Table 3.

Table 2 Grid independence study

Grid number $\times 10^6$	Efficiency η (%)	Error (%)	Head H (m)	Error (%)
3.6	81.23	-	35.39	-
5.8	80.05	1.45	34.89	1.41
7.1	79.52	0.66	34.21	1.95
8.5	79.24	0.35	33.93	0.82
9.4	79.13	0.14	33.68	0.74
10.5	78.9	0.29	33.5	0.53

Table 3 Grid numbers and Y^+ values

Fluid domain	Grid number $\times 10^6$	Average Y^+ value
Inlet pipe	0.66	20.74
Impeller	2.87	55.59
Volute cavity	2.38	28.27
volute	3.28	41.34
Discharge pipe	1.28	22.32

The Ansys commercial software was used to conduct a numerical analysis of the model centrifugal pump. The RANS equation considering a steady condition [20, 23] and the RNG k-ε model were used to analyze the flow in fluid domains [23]. The scalable wall function was used to accurately simulate the near-wall turbulence flow field [21]. The multiple reference frame approach was used for the impeller fluid domain and solved in a rotating frame; whereas the volute, volute cavity, suction pipe, and discharge pipe domains were set as stationary. Water at 25°C was chosen as the fluid medium. The boundary conditions were set as the total pressure at the inlet (1 atm) and mass flow at the outlet (30 kg/s), as expressed in Eqs. (10)-(11), respectively [21].

The velocity inlet normal to the boundary face (0, 0, 1 m/s), isothermal heat transfer, and medium turbulence intensity were set as initial conditions [13]. The connections were defined as frozen for rotor-stator and general for stator-to-stator domains. The no-slip wall was set for the surface of the pump. To consider the wall frictional loss, the standard cast wall

roughness of grade N 12 (sand-grain roughness height = 50 μm) was selected as per ISO 1302 [24]. Surface roughness increases turbulence production near the wall, which is essential for a reasonable agreement with the experimental results [21]. The advection scheme and turbulence numeric were selected as high resolution. In addition, the convergence criterion was set as 1.0E-5 for all equations to achieve precise results.

$$p_{tot} = p_{stat} + \frac{1}{2}\rho U^2 \tag{10}$$

$$\dot{m} = \rho A U \tag{11}$$

4. Experimental Test Setup

The energy performance characteristics of the selected pump were measured on a closed-loop test setup according to ISO 9906 [25], as shown in Fig. 2. The setup comprised a sump, suction-discharge pipe, foot valve, control valve, pressure transducer, electromagnetic flowmeter, rpm sensor, variable frequency drive, and power analyzer. An electric motor with a rated capacity of 415 V, output power of 15 hp, and speed of 2,930 rpm operated the centrifugal pump.
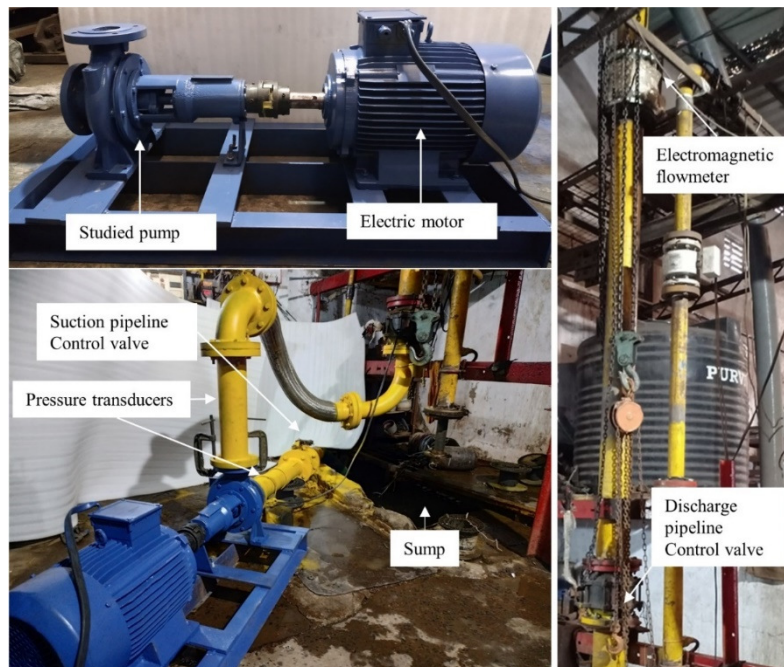
Fig. 2 Experimental setup with the tested centrifugal pump

Measured readings along with errors in the test were as follows: the total pressure head measured by the pressure transducer with a measurement error of ±0.1%, flow measured by the electromagnetic flowmeter with a measurement error of ±0.2%, speed measured by the rpm sensor with a measurement error of ±0.1%, and input power measured by the power analyzer with an overall measurement error of ±0.2%. Thus, the Kline and McClintock uncertainty method [26] was employed to determine the measurement error in overall measured efficiency, which was ±0.80%. The permissible limit in overall measured efficiency was ±4.0% as per ISO 9906 Grade 2 [25]. The repeatability of the test setup was verified using sets of readings; the confidence limit was in a reasonable range of 95%. The numerical results were validated using the experimental results for the base pump model, Vd-40. The graphs of calculated head coefficient and pump efficiency in terms of the flow coefficient were plotted for four different flow rates of 0.6 Q_d, 0.8 Q_d, 1 Q_d, and 1.2 Q_d, as shown in Fig. 3. The empirical law of mechanical and volumetric efficiency, in terms of the pump specific speed, was determined using Eqs. (12)-(13), respectively [27]. The numerical pump efficiency was calculated using Eq. (14) [27]. The dimensional head and flow coefficients were calculated using Eqs. (15)-(16) [27].

$$\frac{1}{\eta_m} = 1 + \frac{820}{n_s^2} \tag{12}$$

$$\frac{1}{\eta_v} = 1 + 0.68 \times n_s^{-0.66} \tag{13}$$

$$\eta_{pump} = \eta_h \times \eta_v \times \eta_m \tag{14}$$

$$\psi = \frac{2gH}{u_2^2} \tag{15}$$

$$\phi = \frac{Q}{\pi d_2 b_2 u_2} \tag{16}$$

(a) Head coefficient versus the flow coefficient   (b) Efficiency versus the flow coefficient
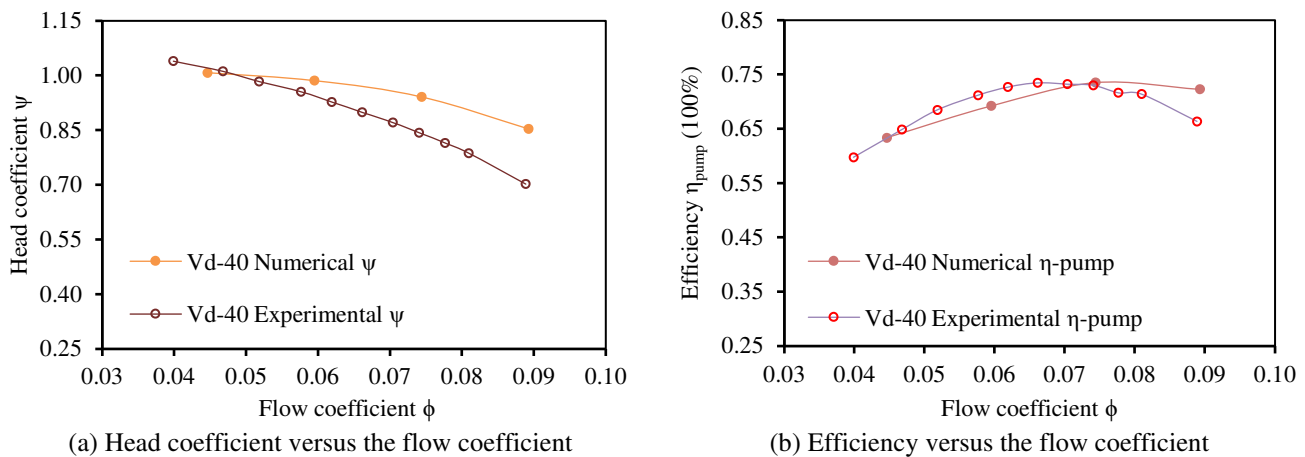
Fig. 3 Comparison of the numerical and experimental results for the base pump model

The results confirmed that increasing the flow rate by regulating the control valve gradually decreases the head owing to the frictional force between the wall and fluid. The head coefficient was primarily affected by the friction losses, whereas the flow coefficient was affected by the leakage losses. According to the numerical and experimental results, the head coefficient decreased with an increasing flow coefficient. The performance curve of the tested base pump model shifted toward the low-flow conditions and was most accurately matched with the numerical and experimental head coefficient. The frictional velocity increases at high flow conditions; therefore, the numerical and experimental head coefficients highly varied under high-flow conditions.

At the duty flow, the numerical and experimental values of the head coefficient were 0.94 and 0.84, respectively. At part and design load conditions, minimal and moderate fluctuations of 0.5 and 9% were achieved in the value of the head coefficient, respectively [7]. In contrast, the pump efficiency exhibited deviations of 0.7, 4, and 8% between the simulation and experimental results for the design load, part load, and overload conditions, respectively [9-10]. At the duty flow, the efficiency and head coefficient deviations were in reasonable ranges. Therefore, the results were acceptable for engineering applications, and numerical results were verified with experiments.

5. Results and Discussion

The single-stage centrifugal pump performance was examined using numerical and experimental analyses for different volute collectors. The flow in machines can be viewed in three-dimensional space using numerical simulation. The calculated quantities were the fields of pressure, velocity, energy loss, and entropy loss coefficient. During the solver iteration, variable quantities, such as the pressure head, efficiency, mass flow rate, and shaft power, were determined. First, the performance curves of the fluid domain for three selected volute collectors were used to compare the obtained results.

The numerical results were determined in the CFD post-processing. An expression was defined to find the values of different variables. The sectional view of the fluid domain, as shown in Fig. 4, was used to examine the flow behavior at various operating conditions. The measuring variables, including viscous dissipation power loss (VDPL), turbulence dissipation power loss (TDPL), wall shear dissipation power loss (WDPL), entropy production, EPC, pump efficiency, head coefficient, and flow coefficient, were calculated using Eqs. (3), (5), (7)-(9), (14)-(16), respectively. Post-processing was essential to verify the simulation results using the experimental data.
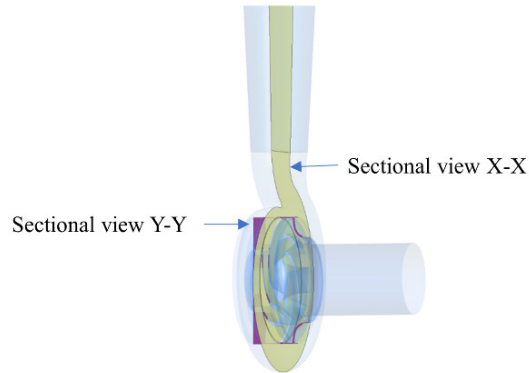
Fig. 4 Sectional view of the fluid domain

5.1. *Numerical simulation results*

The numerically calculated head coefficient and pump efficiency were compared with the flow coefficient for three selected pump models, as shown in Fig. 5. The pressure head of Vd-75 was the highest; it was approximately 18 and 24% higher than that of Vd-50 at the duty flow and under overload conditions, respectively. Moreover, the pressure head of Vd-50 was 2% higher than the base configuration (Vd-40, as presented in Fig. 5(a)) under the design and overload flow conditions. However, the pump efficiency graph revealed the lowest value of efficiency for Vd-75 at all flow coefficients, as demonstrated in Fig. 5(b). At the duty flow, the pump efficiency for Vd-50 and Vd-40 was higher than that of Vd-75 by 9.01 and 6.7%, respectively. Moreover, the pump efficiency of Vd-50 was 2.25% higher than that of Vd-40.

(a) Head coefficient versus the flow coefficient

(b) Efficiency versus the flow coefficient
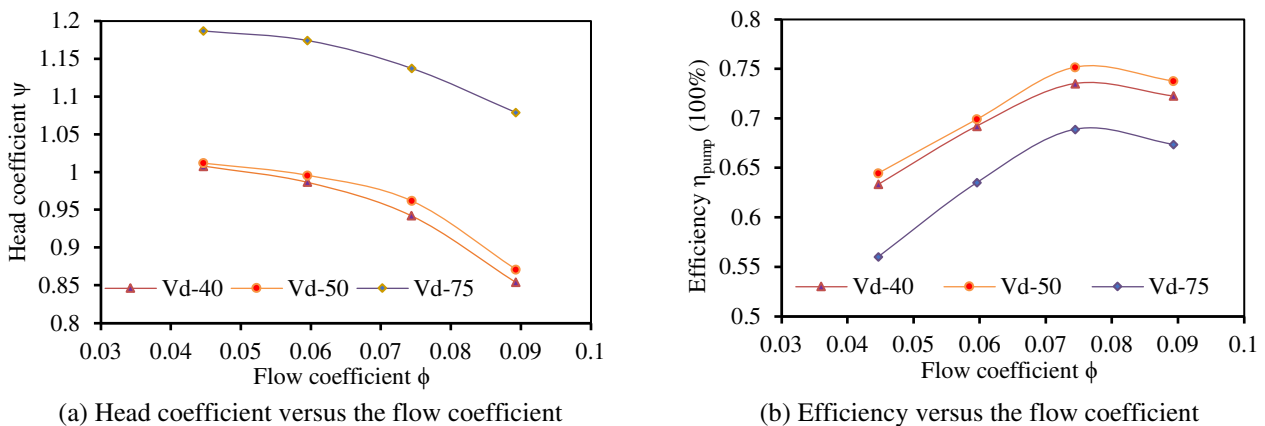
Fig. 5 Comparison of the numerical results for Vd-40, Vd-50, and Vd-75

Furthermore, the cause of energy dissipation by the entropy production method in different flow zones and their effects on subsequent fluid domains must be precisely examined and analyzed. Therefore, contours of the static pressure, the velocity with a vector plot in the local reference frame, and entropy production at the sectional view for the design flow rate of Vd-40, Vd-50, and Vd-75 were plotted, as shown in Figs. 6-10. Moreover, the sectional view X-X and sectional view Y-Y are plotted in Figs. 6-8 and Figs. 9-10, respectively. The contour plots of the static pressure, as presented in Fig. 6, indicated a uniform distribution within the fluid domain for Vd-40 and Vd-50, whereas the static pressure sharply increased across the volute collector for Vd-75. Fig. 7 represents the velocity contours with a vector plot in the local reference frame for fluid domains. It

reveals that a higher velocity was observed across the volute fluid domain of Vd-75 compared to that of Vd-40 and Vd-50. Additionally, the low-velocity zone present in Vd-40 and Vd-50 (A_1, A_2 in Figs. 7(a)-7(b)) diminished in Vd-75 (A_3 in Fig. 7(c)). The results shown in Figs. 6-7 indicate that the Vd-75 configuration is the best fit. Furthermore, to better explore the local energy loss, their effects, and intensity of loss, the contours for entropy production were plotted, as shown in Figs. 8-10.

(a) Vd-40   (b) Vd-50   (c) Vd-75
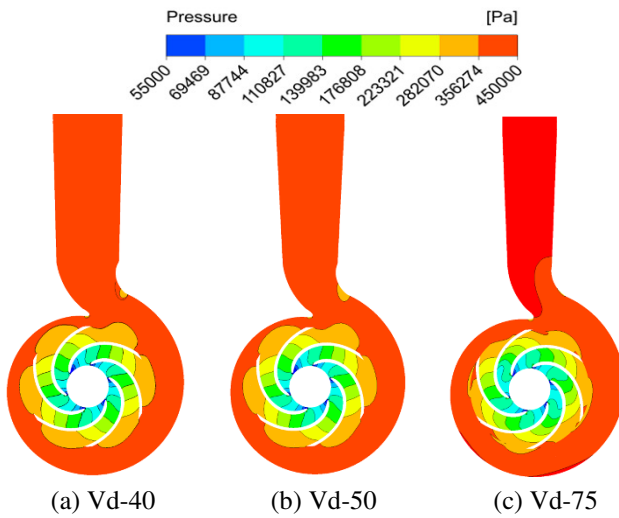
Fig. 6 Static pressure contour

(a) Vd-40   (b) Vd-50   (c) Vd-75
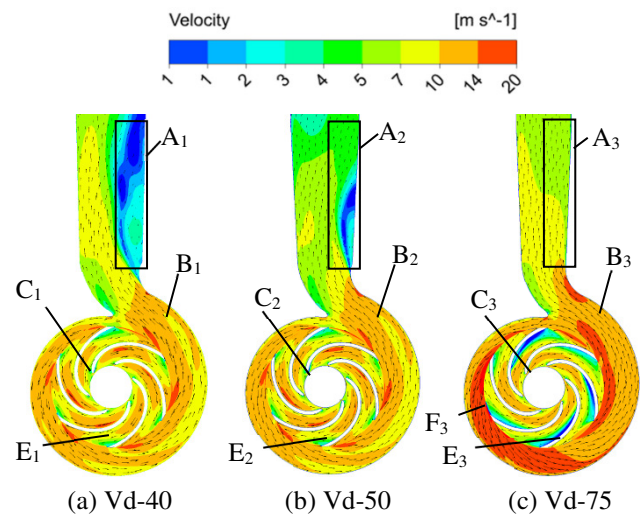
Fig. 7 Velocity contour with a vector plot in the local reference frame

(a) Vd-40   (b) Vd-50   (c) Vd-75
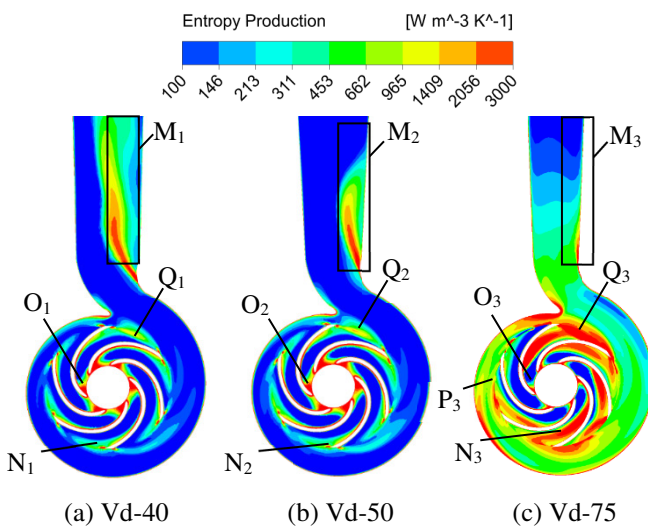
Fig. 8 Entropy production contour

(a) Vd-40   (b) Vd-50   (c) Vd-75
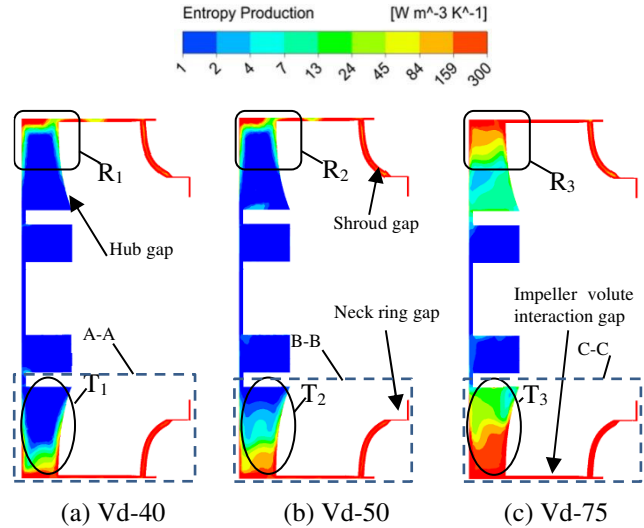
Fig. 9 Entropy production contour in the volute cavity

(a) Vd-40   (b) Vd-50   (c) Vd-75
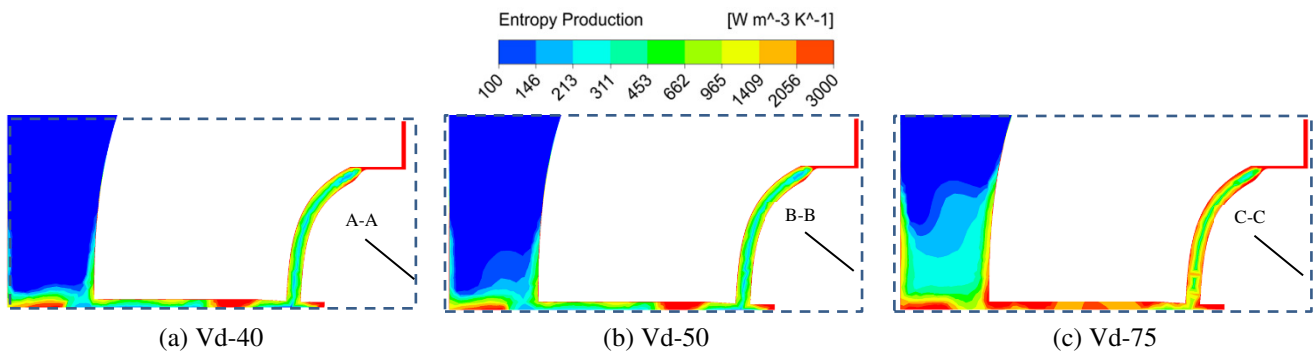
Fig. 10 Entropy production contour in the volute cavity (sections A-A, B-B, and C-C of Fig. 9)

An examination of the flow across the pump assembly at the sectional view revealed a reasonable agreement between the relative velocity distribution and energy dissipation. As the intensity of velocity varied, the entropy production increased [6]. The suction area of impeller blades indicated a low velocity at the leading edge to weak inlet flow velocities [10] (C_1, C_2, C_3

in Figs. 7(a)-7(c)). A low relative velocity, owing to the flow separation at the trailing edge suction face of the impeller blade, was observed (E_1, E_2, E_3 in Figs. 7(a)-7(c)), which increased the entropy in the fluid domain (O_1, O_2, O_3, N_1, N_2, N_3, in Figs. 8(a)-8(c)). A weak velocity was observed owing to the flow separation (A_1, A_2 in Figs. 7(a)-7(b)), which produced an entropy (M_1, M_2 in Figs. 8(a)-8(b)). Furthermore, the flow separation disappeared (A_3, Fig. 7(c)) and the entropy production was reduced (M_3, Fig. 8(c)) in the discharge pipe of Vd-75 [6].

The reduced discharge diameter of the volute (Vd-75) predominantly increased the flow velocity (F_3, Fig. 7(c)) in the downstream domain [13]. Moreover, the increased flow velocity further disturbed the flow and raised the entropy at the impeller and volute fluid domains (P_3, Fig. 8(c)). The impeller losses increased by reducing the discharge diameter of the volute.

The entropy production was more than 2,000 W/(m^3·K) at the inflow (O_1, O_2, Figs. 8(a)-8(b)) and outflow (M_1, M_2, Figs. 8(a)-8(b)) regions of the pump owing to the low fluid velocity at the impeller inlet and flow separation of the volute outlet. The fluid at the impeller-volute interaction zone increased the entropy production up to 1,500 W/(m^3·K) (N_1, N_2, Figs. 8(a)-8(b)). The trailing edge and suction surface of the impeller blade profile contributed to higher losses in all three cases. Owing to the reduction in the volute discharge diameter, losses were marginally and significantly increased in Vd-50 and Vd-75 compared to those of Vd-40, respectively. According to a study conducted by Shah et al. [28], as the fluid flow leaves the impeller passage near the volute tongue regions, the volume of fluid collides with the volute wall and fluid leaving the volute, resulting in a vortex. An entropy loss was generated owing to the vortex formation (Q_1, Q_2, Q_3, Figs. 8(a)-8(c)). The wall shear has a significant effect on the total energy dissipation loss, which is measured by entropy production. The frictional effect between the fluid flow and wall is accountable for the entropy production by the wall shear.

The volute cavity is a noneffective flow zone in the centrifugal pump assembly. The clearance gap between the rotating and stationary parts in a centrifugal pump is covered by the volute cavity domain, as shown in Fig. 9. The shroud gap and hub gap were designed as small as possible to reduce entropy production. However, the shroud gap contributed more entropy production than the hub gap. The entropy production was visualized at the impeller volute interaction zone owing to the fluid leaving the rotating domain and entering the stationary domain, as presented in Figs. 9-10. The energy loss intensity at the outer periphery of the hub gap was higher owing to the fluid entering from the impeller (R_1, R_2, R_3, T_1, T_2, T_3, Figs. 9(a)-9(c)). The entropy production was more at the neck ring gap owing to the pressure difference between the suction and impeller outflow pressures, as shown in Fig. 10.

Thus, comparing the simulation results of the three volute collectors suggests that despite a high head coefficient at different flow rates, the efficiency of Vd-75 reduces owing to higher entropy production and losses. However, Vd-50 exhibited a better head and efficiency with comparable entropy production and losses of Vd-40.

5.2. Total entropy production

Additionally, the entropy production in Vd-50 at the duty and off-duty flows was analyzed. In hydro turbomachinery, the dissipation of power loss by fluid dynamics is the primary cause of entropy generation. Comparable trends of the hydraulic power loss (P_{loss}) and total energy loss (TEL) were observed owing to the entropy generation, as shown in Fig. 11(a). The power loss at the duty flow was less than that at the off-duty flow, as presented in Fig. 11(a). The ratio of the input power to the energy loss was minimum (6.4%) at the flow rates of 1.0 and 1.2 Q_d. Moreover, the gap increased by a maximum of 7.8 and 8% for flow rates of 0.8 and 0.6 Q_d, respectively. The minimum gap and similar trends in the energy loss validated the entropy production methods to analyze the energy loss in various fluid domains of centrifugal pumps [7].

The entropy production methods suggest that TDPL and VDPL are present in the main flow regions that can be calculated using Eq. (6), whereas WDPL is present near the wall areas that are calculated using Eq. (7). The summation of TDPL, VDPL,

and WDPL results in total energy loss in the fluid domain that can be calculated using Eq. (8). The flow reversal, wake flow, and vortex are the primary reasons for the turbulent kinetic energy dissipation. Furthermore, the viscous effect and wall frictions are the primary causes of the viscous and wall shear dissipations, respectively.

Fig. 11(b) shows the dissipation power loss owing to the entropy production across the flow field in various fluid domains under the design and off-design flow conditions. Moreover, WDPL in the main flow regions (impeller, volute, and volute cavity) was relatively constant and marginally increased with the flow rate. It was below 50 W in the suction and discharge pipe regions and below 250 W in the main flow regions of the model pump. Thus, the flow rate change has an insignificant effect on the wall shear stress and velocity near the wall. The entropy generation in the main flow region was higher than that in the wall regions.

(a) Energy loss versus the mass flow   (b) Dissipation power loss versus the mass flow
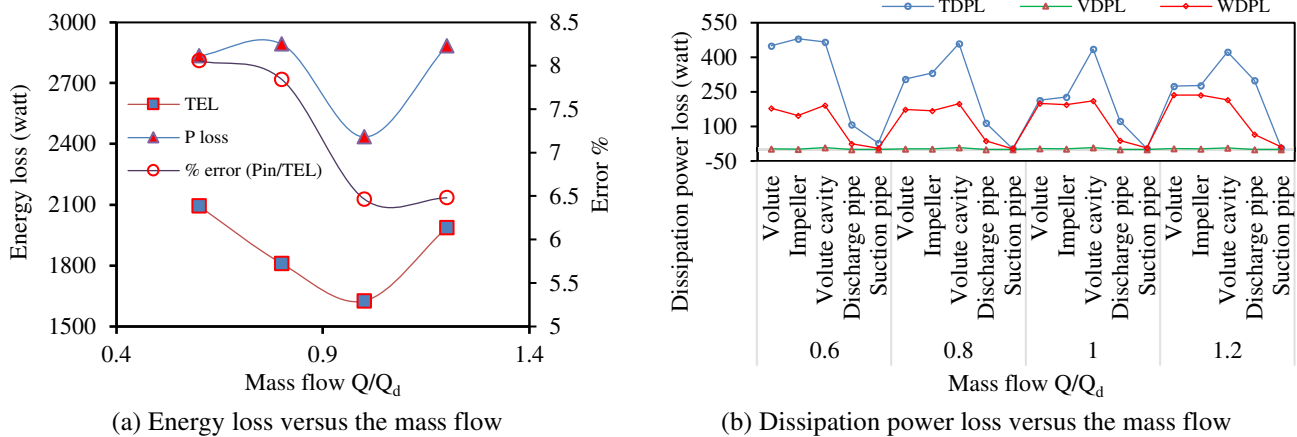
Fig. 11 Energy loss analysis for Vd-50

TDPL is inversely proportional to the flow rate; thus, an increasing flow rate decreases TDPL. The main flow regions of the pump significantly increase TDPL. Indeed, the volute cavity represents the highest losses owing to the nonguided flow. Moreover, the volute and impeller equally contribute to the development of TDPL. In this study, the TDPL value at 0.6 Q_d was double that of 1.0 Q_d in the impeller and volute fluid domains. The volute losses were less than those of the impeller losses in the range of 0.6-1 Q_d, whereas they were equal at 1.2 Q_d.

Although insignificant changes were observed in the volute cavity flow regions under different flow conditions, the volute cavity exhibited an approximately constant dissipation power loss of 460 W under the part load (0.6 and 0.8 Q_d) and 430 W under the design and overload (1 and 1.2 Q_d) flow conditions, as presented in Fig. 11(b). TDPL was the lowest under the design and the highest under off-design flow conditions for all fluid domains, except for the discharge pipe. The discharge pipe exhibited approximately constant losses in the range of 0.6-1 Q_d, which significantly increased at 1.2 Q_d by 30 W. However, an increase in the flow rate increased the flow separation near the volute outlet and extended up to the discharge pipe fluid domain. These dissipation losses emerged owing to the combined effect of the volute and discharge pipe fluid domains. In addition, VDPL insignificantly contributed to the total energy loss for all domains over the entire flow range of the model pump [10, 20].

Fig. 12(a) presents the entropy generation in the main flow field for each domain at a different flow rate. The TEL value was the highest in the volute cavity for the full flow range of the model pump; it was 667 W at 0.6 Q_d and reduced to 645 W at 1.2 Q_d. Fig. 12(b) shows that TEL in the volute cavity has the highest (40%) contribution to the energy loss at the duty flow and the lowest (32%) for 0.6 and 1.2 Q_d. The total energy loss in the volute and impeller exhibits a similar trend as the power loss, that is, high at 0.6 Q_d and low at the duty flow, as shown in Fig. 12(a) [12].

Furthermore, Fig. 12(b) reveals that energy loss has an equal proportion rate of 30% for the volute and impeller at 0.6 Q_d. The impeller exhibits a consistent proportion of 26% in the energy loss contribution in the range of 0.8-1.2 Q_d, whereas the

proportion of TEL in the volute decreases with an increasing flow rate. The entropy production was primarily affected by the volute cavity, volute, and impeller. The discharge pipe exhibited an increase in TEL with an increasing flow rate; it increased up to three times at 1.2 Q_d compared with that at 0.6 Q_d. The suction pipe indicates approximately 1% of the proportion contribution for the flow rate under the design and off-design conditions.

(a) Total energy loss versus the mass flow   (b) Energy loss versus the mass flow
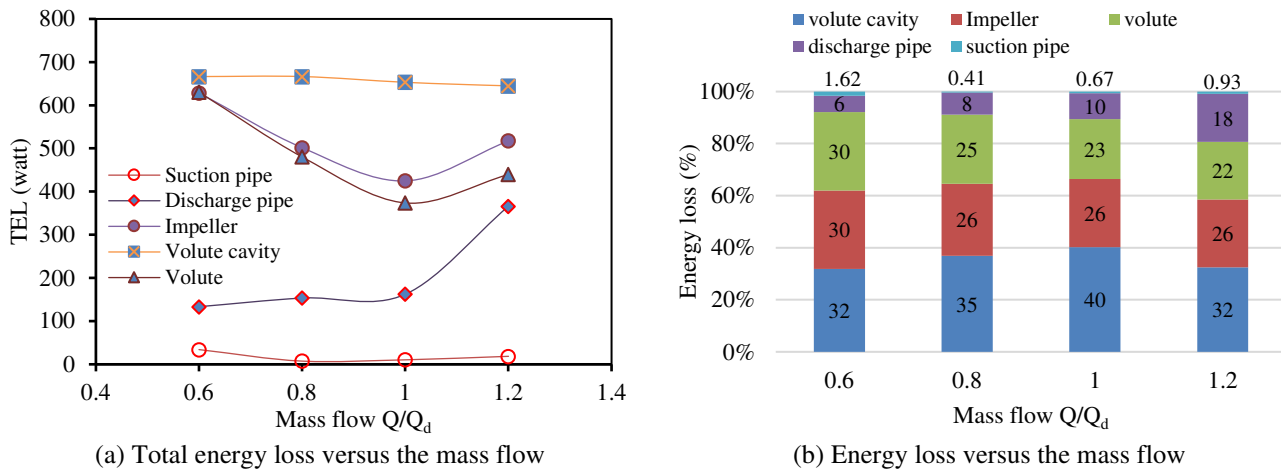
Fig. 12 Total energy loss in different domains for Vd-50

5.3.   *Comparison of total energy loss and total pressure loss*

In hydraulic machines, efficiency is the most crucial aspect of performance measured under the design and off-design conditions. The total pressure difference between the inlet and outlet of the domain evaluates the power loss of each domain and determines the hydraulic efficiency. The power loss in the stationary and rotating domains is calculated using Eqs. (17)-(18), respectively [5-6, 9]. The energy loss calculated using the entropy production method was used to compare the TPL of the domains. Fig. 13 shows a comparison between TPL and TES for Vd-40, Vd-50, and Vd-75 at different volute collector area ratios and mass flow variations of 0.6, 0.8, 1, and 1.2 Q_d.

$$TPL\left(stationary\right) = \int_{in} P_{tot}\,dQ - \int_{out} P_{tot}\,dQ \tag{17}$$

$$TPL\left(rotating\right) = W_s - (\int_{out} P_{tot}\,dQ - \int_{in} P_{tot}\,dQ) \tag{18}$$

$$TPLC\left(rotating\right) = \frac{P_{rel,\,tot,\,in} - P_{rel,\,tot}}{P_{rel,\,tot,\,in} - P_{rel,\,tot,\,out}} \tag{19}$$

The TPL value was higher in the impeller and lower in the volute cavity compared to the TES value [9, 12]. The difference between TPL and TES was less in the fluid domains, namely, the volute, suction pipe, and discharge pipe [13]. TPL of the fluid domains was equivalent to the energy loss of that domain; it was ideally used to calculate the hydro efficiency of turbomachines. However, it could not identify the influence of local losses in the fluid domain.

Therefore, the TEL calculated using the entropy production methods was utilized in the quantitative analysis. In addition to this, the power loss of the fluid domain defined by TEL was 70-80% of that defined by TPL [9]. Thus, conducting studies on TPL and TEL is crucial. In this study, TPL helps determine the overall losses across the fluid domain, whereas TEL measured using the entropy production method defines the intensity of local losses. Therefore, the entropy production method is a useful tool to determine the modified volute collector area ratio of the model centrifugal pump. However, the calculated loss values significantly affect the upstream and downstream fluid domains. The power loss in the volute cavity determined by TPL was approximately 30-40% of that defined by TEL. The power loss in the suction pipe domain is less, whereas it was high in the discharge pipe domain. Moreover, TEL and TPL were approximately the same in the suction and discharge pipe fluid domains.

(a) Impeller

(b) Volute

(c) Volute cavity

(d) Suction pipe

(e) Discharge pipe
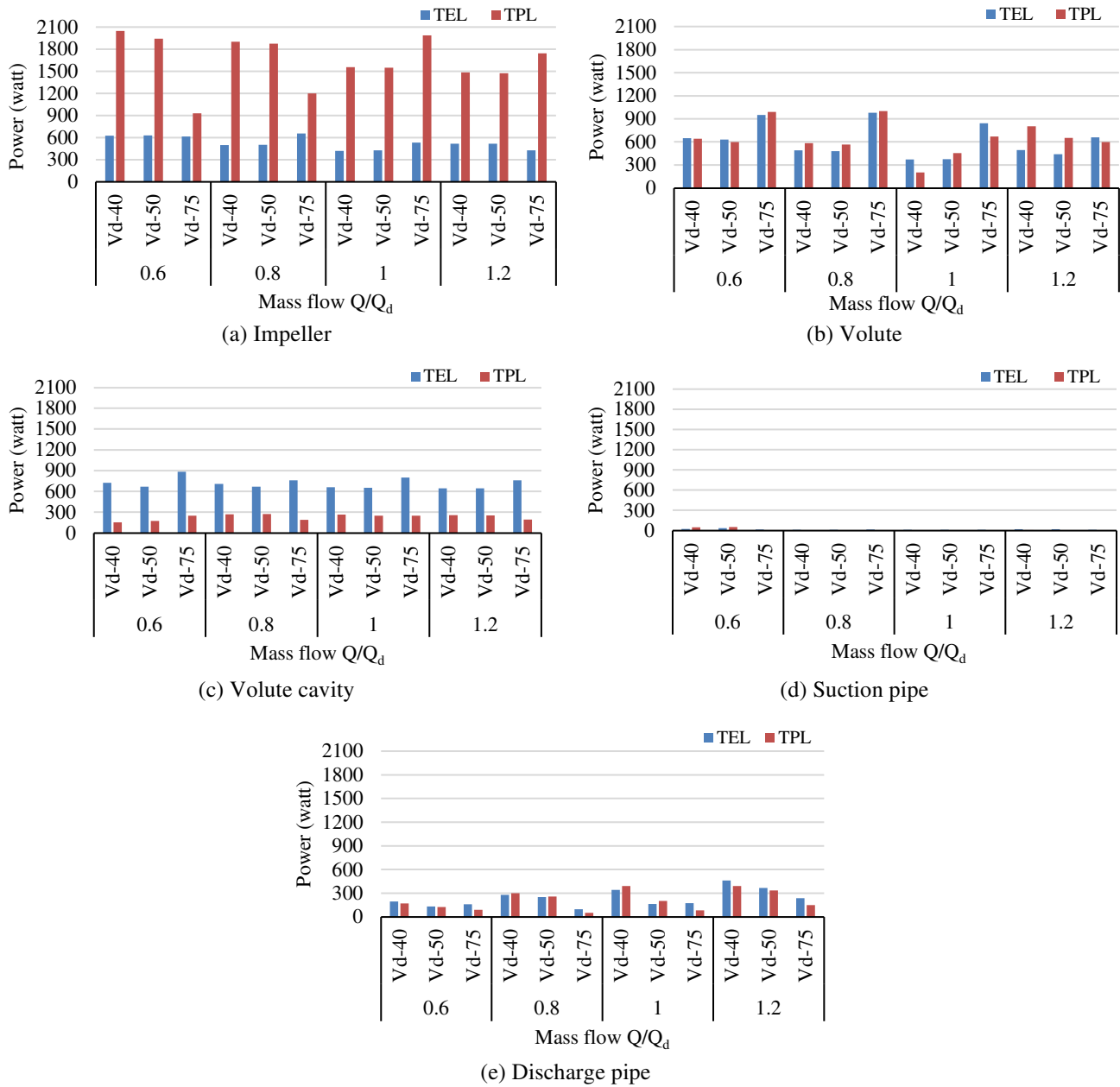
Fig. 13 Comparison of the total energy loss and total pressure loss for all domains at various mass flows

Fig. 13 demonstrates more total pressure losses inside the impeller compared to other components of the fluid assembly. To gain more insight into the flow losses within the impeller, variations of the relative total pressure loss coefficient were plotted for different mass flow rates in the relative reference frame, as shown in Fig. 14. The value of TPLC can be calculated using Eq. (19) [29]. Fig. 14 illustrates minor deviations in the relative TPLC of the rotating frame for different volute collector configurations.
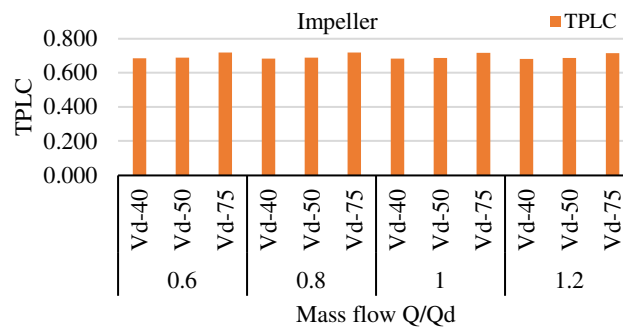
Fig. 14 Relative total pressure loss coefficient in the relative reference frame

5.4. Results of the experimental analysis

The numerical simulation results suggest that less energy loss in Vd-50 existed. Therefore, the pump with a discharge diameter of the volute collector of 80 mm (Vd-50) was developed to conduct the experimental analysis. The experiments were performed as per ISO 9906 for a complete operating range of the centrifugal pump, that is, from the shut-off condition to the full opening of the discharge valve at the rated speed [25]. According to the experimental results, the performance characteristics were plotted in a non-dimensional form for the head coefficient in addition to the pump efficiency concerning the flow coefficient, as shown in Figs. 15-16.
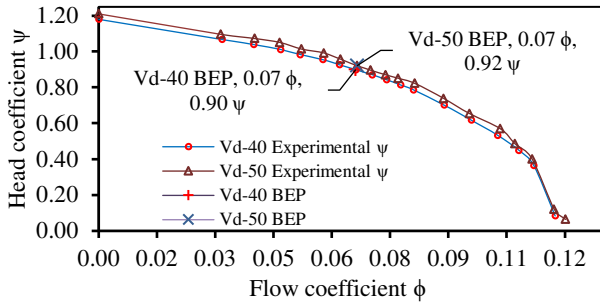
Fig. 15 Head coefficient variations versus
the flow coefficient
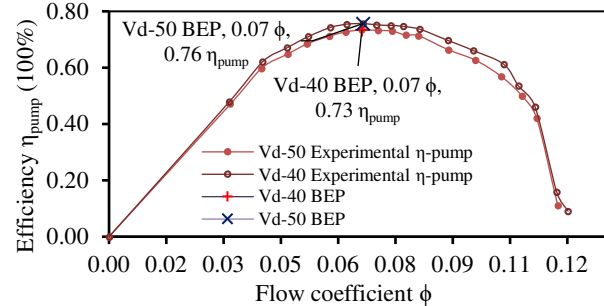
Fig. 16 Pump efficiency variations versus
the flow coefficient

Fig. 15 demonstrates that the head coefficient in Vd-50 is better than that of Vd-40 for the entire operating range of the model centrifugal pump. At the best efficiency point (BEP), the value of the head coefficient in Vd-50 increased by 2.22%, that is, from 0.90 to 0.92. Fig. 16 illustrates the pump efficiency at different flow rates. The efficiency of Vd-50 was higher than that of Vd-40 under the part load and overload flow conditions, except for the flow near the shut-off and maximum flow conditions. At BEP, Vd-50 yielded an efficiency of 76%, whereas that of Vd-40 was 73%. These enhancements indicate less energy loss in Vd-50 compared to Vd-40.

The numerical results proved that a modified volute collector design helps maintain the vortex formation and reduces the secondary flow losses within the volute collector and discharge pipe fluid domains. Thus, the overall performance of the centrifugal pump can be enhanced. Consequently, the authors believe that selecting one commercial size lower volute discharge diameter than the designed one helps increase the pump performance.

6. Summary and Conclusions

This study was conducted using a steady-state numerical simulation of the centrifugal pump with three different volute collector area ratios. In addition, it did not incorporate the unsteady nature of the flow. According to the numerical results, the modified configuration of the volute collector was developed. Subsequently, the experimental performance of the modified volute collector was compared with that of the base volute collector. The following conclusions were drawn:

(1) The numerical and experimental results for the base pump model, Vd-40, revealed that an increased flow rate gradually decreased the head owing to the frictional force between the wall to fluid and in the fluid itself. The pump efficiency deviated 0.7, 4, and 8% between the numerical to experimental results under the design load, part load, and overload conditions, respectively. At the duty flow, deviations in the efficiency and head coefficient were in a reasonable range.

(2) Numerical results suggested that the primary causes for the energy dissipation were likely the turbulence, viscous, and wall shear effects in the flow field. The losses in the impeller and volute cavities increased with an increase in the volute collector area ratio, which resulted in a high flow velocity, friction loss, and flow restriction in the volute collector. Thus, the proper design of the volute collector can enhance the efficiency by reducing the secondary flow losses over the entire operating flow range of the model pump.

(3) The reduced discharge diameter of Vd-75 predominantly increased the flow velocity. The increased flow velocity developed more disturbance in the flow and raised the entropy at the impeller and volute fluid domain. Moreover, Vd-50 exhibited a better head and efficiency than those of Vd-40, whereas the entropy production and losses were comparable. Thus, the proper design of the volute collector is essential in the reduction of the entropy production and losses within the centrifugal pumps. The experimental analysis demonstrated an improvement of 3% in the efficiency of the modified volute collector, Vd-50. In addition, the numerical simulation results proved a reduction of 9.5% in the energy losses compared to those of Vd-40.

Nomenclature

CFD	Computational fluid dynamics	q	Heat transfer
EPC	Entropy production coefficient	d_1	Impeller suction eye diameter (mm)
Y^+	Dimensional distance from the wall	d_2	Impeller outlet diameter (mm)
Q	Volume flow rate (m³/s)	b_1	Impeller inlet width (mm)
RANS	Reynolds averaged navier stokes	b_2	Impeller outlet width (mm)
RNG	Renormalization group	β_1	Impeller blade inlet angle (°)
k	Turbulence kinetic energy (m²/s²)	β_2	Impeller blade outlet angle (°)
ε	Turbulence eddy dissipation (m²/s³)	φ	Impeller blade wrap angle (°)
μ	Dynamic viscosity (kg/m·s)	Z	Impeller blade number (nos.)
ψ	Head coefficient	δ	Impeller blade thickness (mm)
ϕ	Flow coefficient	n_l	Length of impeller neck ring (mm)
P_{EP}	Power loss by entropy (W)	d_3	Volute base diameter (mm)
P_w	Power loss by wall shear (W)	b_3	Volute inlet width (mm)
P_t	Total power loss (W)	φ_o	Volute tongue angle (°)
VFD	Variable frequency drive	d_4	Volute outlet diameter (mm)
TEL	Total energy loss (W)	H	Head (m)
TDPL	Turbulence dissipation power loss (W)	u_2	Peripheral velocity
VDPL	Viscous dissipation power loss (W)	n_s	Specific speed of pump
WDPL	Wall shear dissipation power loss (W)	η_h	Hydraulic efficiency
TPL	Total pressure loss (W)	η_v	Volumetric efficiency
BEP	Best efficiency point	η_m	Mechanical efficiency
s	Specific entropy (m²/s²·K)	Q_d	Nominal (design) flow rate (m³/s)
λ	Thermal conductivity (W/m·K)	V_d	Volute collector area ratio (Vd-40, Vd-50, Vd-75)
Φ, Φ_θ	Dissipation function	τ_w	Wall shear stress (kg/m·s²)
U (u, v, w)	Cartesian velocity components	v_w	Near wall velocity (m/s)
x, y, z	Cartesian coordinate components	ω	Angular velocity (1/s)
$\Phi_{D'}$	Indirect or turbulent dissipation	ρ	Density of fluid (kg/m³)
$\Phi_{\bar{D}}$	Direct or viscous dissipation	T	Temperature (K)
A	Area (m²)	g	Gravitational constant (m/s²)
P_{tot}	Total pressure (kg/m·s²)	$\dot{m}$	Mass flow rate (kg/s)
P_{stat}	Static pressure (kg/m·s²)	W_s	Shaft input power (W)

Acknowledgments

Conflicts of Interest

The authors declare no conflict of interest.

References

[1] C. Wang W. D. Shi, X. K. Wang, X. P. Jiang, Y. Yang, W. Li, et al., "Optimal Design of Multistage Centrifugal Pump Based on the Combined Energy Loss Model and Computational Fluid Dynamics," Applied Energy, vol. 187, pp. 10-26, February 2017.

[2] Y. Hao and L. Tan, "Symmetrical and Unsymmetrical Tip Clearances on Cavitation Performance and Radial Force of a Mixed Flow Pump as Turbine at Pump Mode," Renewable Energy, vol. 127, pp. 368-376, April 2018.

[3] F. Kock and H. Herwig, "Entropy Production Calculation for Turbulent Shear Flows and their Implementation in CFD Codes," International Journal of Heat and Fluid Flow, vol. 26, no. 4, pp. 672-680, June 2005.

[4] M. Bhole, C. Ford, and J. Bennington, "Characterization of Axial Flow Impellers in Pulp Fibre Suspensions," Chemical Engineering Research and Design, vol. 87, pp. 648-653, April 2009.

[5] G. Hongyu, J. Wei, W. Yuchuan, T. Hui, L. Ting, and C. Diyi, "Numerical Simulation and Experimental Investigation on the Influence of the Clocking Effect on the Hydraulic Performance of the Centrifugal Pump as Turbine," Renewable Energy, vol. 168, pp. 21-30, 2021.

[6] Y. D. Gu, J. Pei, S. Q. Yuan, W. J. Wang, F. Zhang, P. Wang, et al., "Clocking Effect of Vaned Diffuser on Hydraulic Performance of High-Power Pump by using the Numerical Flow Loss Visualization Method," Energy, vol. 170, pp. 986-997, March 2019.

[7] H. Guan, W. Jiang, J. Yang, Y. Wang, X. Zhao, and J. Wang, "Energy Loss Analysis of the Double-Suction Centrifugal Pump Under Different Flow Rates Based on Entropy Production Theory," Proceedings of the Institution of Mechanical Engineers, Part C: Journal of Mechanical Engineering Science, vol. 234, no. 20, pp. 4009-4023, April 2020.

[8] Q. Deng, J. Pei, W. Wang, B. Lin, C. Zhang, and J. Zhao, "Energy Loss and Radial Force Variation Caused by Impeller Trimming in a Double-Suction Centrifugal Pump," Entropy, vol. 23, no. 9, article no. 1228, September 2021.

[9] F. Zhang, D. Appiah, F. Hong, J. F. Zhang, S. Q. Yuan, K. A. Adu-Poku, et al., "Energy Loss Evaluation in a Side Channel Pump under Different Wrapping Angles using Entropy Production Method," International Communications in Heat and Mass Transfer, vol. 113, article no. 104526, April 2020.

[10] P. Huang, D. Appiah, K. Chen, F. Zhang, P. Cao, and Q. Hong, "Energy Dissipation Mechanism of a Centrifugal Pump with Entropy Generation Theory," AIP Advances, vol. 11, no. 4, article no. 045208, April 2021.

[11] G. J. Peng, J. L. Du, H. Chang, Q. Chen, J. H. Li, C. X. Pan, et al., "Numerical and Experimental Analysis of Influence of Impeller Structures on Slurry Pump Performance," Frontiers in Energy Research, vol. 9, article no. 762159, November 2021.

[12] F. Yang, Z. B. Li, W. Z. Hu, C. Liu, D. J. Jiang, D. S. Liu, et al., "Analysis of Flow Loss Characteristics of Slanted Axial-Flow Pump Device Based on Entropy Production Theory," Royal Society Open Science, vol. 9, no. 1, article no. rsos.211208, January 2022.

[13] J. Li, D. Meng, and X. Qiao, "Numerical Investigation of Flow Field and Energy Loss in a Centrifugal Pump as Turbine," Shock and Vibration, vol. 2020, article no. 8884385, 2020.

[14] G. Yang, X. Zhao, D. Zhang, L. Geng, X. Yang, and X. Gao, "Hydraulic Components' Matching Optimization Design and Entropy Production Analysis in a Large Vertical Centrifugal Pump," Journal of Mechanical Science and Technology, vol. 35, no. 11, pp. 5033-5048, October 2021.

[15] B. Cui and C. Zhang, "Investigation on Energy Loss in Centrifugal Pump Based on Entropy Generation and High-Order Spectrum Analysis," Journal of Fluids Engineering, Transactions of the ASME, vol. 142, no. 9, article no. 091205, September 2020.

[16] L. Ji, W. Li, W. Shi, H. Chang, and Z. Yang, "Energy Characteristics of Mixed-Flow Pump Under Different Tip Clearances Based on Entropy Production Analysis," Energy, vol. 199, article no. 117447, May 2020.

[17] F. Kock and H. Herwig, "Local Entropy Production in Turbulent Shear Flows: A High-Reynolds Number Model with Wall Functions," International Journal of Heat and Mass Transfer, vol. 47, no. 10-11, pp. 2205-2215, May 2004.

[18] L. Zhou, J. W. Hang, L. Bai, Z. Krzemianowski, M, A, El-Emam, E. Yasser, et al., "Application of Entropy Production Theory for Energy Losses and Other Investigation in Pumps and Turbines: A Review," Applied Energy, vol. 318, article no. 119211, July 2022.

[19] M. Böhle, A. Fleder, and M. Mohr, "Study of the Losses in Fluid Machinery with the Help of Entropy," 16th International Symposium on Transport Phenomena, and Dynamics of Rotating Machinery, April 2016.

[20] H. Hou, Y. Zhang, and Z. Li, "A Numerical Research on Energy Loss Evaluation in a Centrifugal Pump System Based on Local Entropy Production Method," Thermal Science, vol. 21, no. 3, pp. 1287-1299, 2017.

[21] "User's Guide: ANSYS CFX-Solver Theory Guide," https://download.ansys.com/Product%20Documentation, 2022.

[22] "User's Guide: ANSYS CFX-Solver Modeling Guide," https://download.ansys.com/Product%20Documentation, 2022.

[23] C. Wang, Y. Zhang, H. Hou, J. Zhang, and C. Xu, "Entropy Production Diagnostic Analysis of Energy Consumption for Cavitation Flow in a Two-Stage LNG Cryogenic Submerged Pump," International Journal of Heat and Mass Transfer, vol. 129, pp. 342-356, February 2019.

[24] Geometrical Product Specifications (GPS) - Indication of Surface Texture in Technical Product Documentation, ISO 1302, 2002.

[25] Rotodynamic Pumps - Hydraulic Performance Acceptance Tests - Grades 1 and 2, ISO 9906, 2012.

[26] S. Kline and F. Mcclintock, "Describing the Uncertainties in Single Sample Experiments," Mechanical Engineering, vol. 75, pp. 3-8, 1953.

[27] K. M. Srinivasan, Rotodynamic Pumps: (Centrifugal and Axial), New Age International, 2008.

[28] M. Shah, B. Baloni, and S. Channiwala, "Optimization of Centrifugal Pump Based on Impeller-Volute Interactions," Advances in Technology Innovation, vol. 7, no. 3, pp. 216-227, June 2022.

[29] P. Chen, X. Li, J. Ren, and H. Jiang, "Multi-Objective Optimization of Non-Axisymmetric Contoured Endwall for Axial Turbines," International Journal of Gas Turbine, Propulsion and Power Systems, vol. 12, no. 1, pp. 1-9, 2021.